

Towards Visible Soliton Microcomb Generation

Seung Hoon Lee^{1*}, Dong Yoon Oh^{1*}, Qi-Fan Yang^{1*}, Boqiang Shen^{1*}, Heming Wang^{1*},
Ki Youl Yang¹, Yu Hung Lai¹, Xu Yi¹, and Kerry Vahala^{1†}

¹T. J. Watson Laboratory of Applied Physics, California Institute of Technology, Pasadena, California 91125, USA.

*These authors contributed equally to this work.

†Corresponding author: vahala@caltech.edu

Frequency combs have applications that now extend from the ultra-violet into the mid infrared bands. Microcombs¹, a miniature and often semiconductor-chip-based device, can potentially access most of these applications, but are currently more limited in spectral reach. Here, we demonstrate mode-locked silica microcombs with emission near the edge of the visible spectrum. By using both geometrical and mode-hybridization dispersion control, devices are engineered for soliton generation while also maintaining optical Q factors as high as 80 million. Mode locking occurs with threshold powers as low as 5.4 mW despite the larger resonator diameters required to attain electronics-bandwidth-compatible soliton repetition-rates. These are the shortest wavelength soliton microcombs demonstrated to date and could be used in miniature time standards based upon the 2-photon clock transition at 778 nm in rubidium². The results should extend to visible and potentially ultraviolet bands for additional clock transitions³ and application to precision spectroscopy^{4,5}.

Soliton microcombs^{6–10} provide a pathway to miniaturize many conventional comb applications. They have also opened investigations into new nonlinear physics associated with dissipative Kerr solitons⁶ and Stokes solitons¹¹. In contrast to early microcombs, soliton microcombs eliminate instabilities, provide stable (low-phase-noise) mode locking and feature a highly reproducible spectral envelope. Many applications of these devices are being studied including chip-based optical frequency synthesis¹², secondary time standards² and dual-comb spectroscopy^{13–15}. Also, a range of operating wavelengths is opening up by use of several low-optical-loss dielectric materials for resonator fabrication. In the near-infrared (IR), microcombs based on magnesium fluoride⁶, silica^{7,16} and silicon nitride^{8–10,17,18} are being studied for frequency metrology and frequency synthesis. In the mid-IR spectral region silicon nitride¹⁹, crystalline²⁰, and silicon-based²¹ Kerr microcombs as well as quantum-cascade microcombs²² are being studied for application to molecular fingerprinting. At shorter wavelengths below 1 μm , microcomb technology would benefit optical atomic clock technology³ as well as precision spectroscopy^{4,5} and remote sensing spectroscopy²³. Efforts directed towards short wavelength microcomb operation include 1 μm microcombs in

silicon nitride microresonators²⁴ as well as harmonically-generated combs. The latter have successfully converted near IR comb light to shorter wavelength bands²⁵ and even into the visible band^{26,27} within the same resonator used to create the initial comb of near-IR frequencies. Finally, diamond-based microcombs afford the possibility of wide wavelength coverage²⁸. However, none of the short wavelength microcomb systems have so far been able to generate stable mode-locked microcombs as required in all comb applications.

A key impediment to mode-locked microcomb operation at short wavelengths is material dispersion associated with the various dielectric materials used for microresonator fabrication. At shorter wavelengths, these materials feature large normal dispersion that dramatically increases into the visible and ultraviolet bands. Soliton-based mode-locking, on the other hand, requires anomalous dispersion. Dispersion engineering by proper design of the resonator geometry^{29–34} offers a possible way to offset the normal dispersion. Typically, by compressing a resonator's waveguide dimension, geometric dispersion will ultimately compensate a large normal material dispersion component to produce overall anomalous dispersion. For example, in silica, strong confinement in straight waveguides has been used to push the anomalous dispersion transition wavelength into the visible band³⁵. However, to compensate the rising material dispersion this compression must increase as operational wavelength is decreased, and as a side effect highly-confined waveguides tend to suffer increased optical losses. This happens because mode overlap with the etched surface and the cladding is greater with reduced waveguide cross section. Increasing optical loss degrades the resonator Q factor and increases pumping power since the comb threshold power varies inverse quadratically with Q factor³⁶.

Minimizing material dispersion provides one way to ease the impact of these constraints. In this sense, silica offers an excellent material for short wavelength operation, because it has the lowest dispersion among all on-chip integrable materials. For example, at 778 nm, silica has a group velocity dispersion (GVD) equal to 38 ps^2/km . This is over 5X smaller than the GVD of silicon nitride at this wavelength ($> 200 \text{ ps}^2/\text{km}$)³⁷. Other integrable materials that are also transparent in the visible, such as diamond²⁸ and aluminum nitride³⁸, have dispersion that is similar to or even higher than silicon nitride. Silica also features a spectrally-broad low-

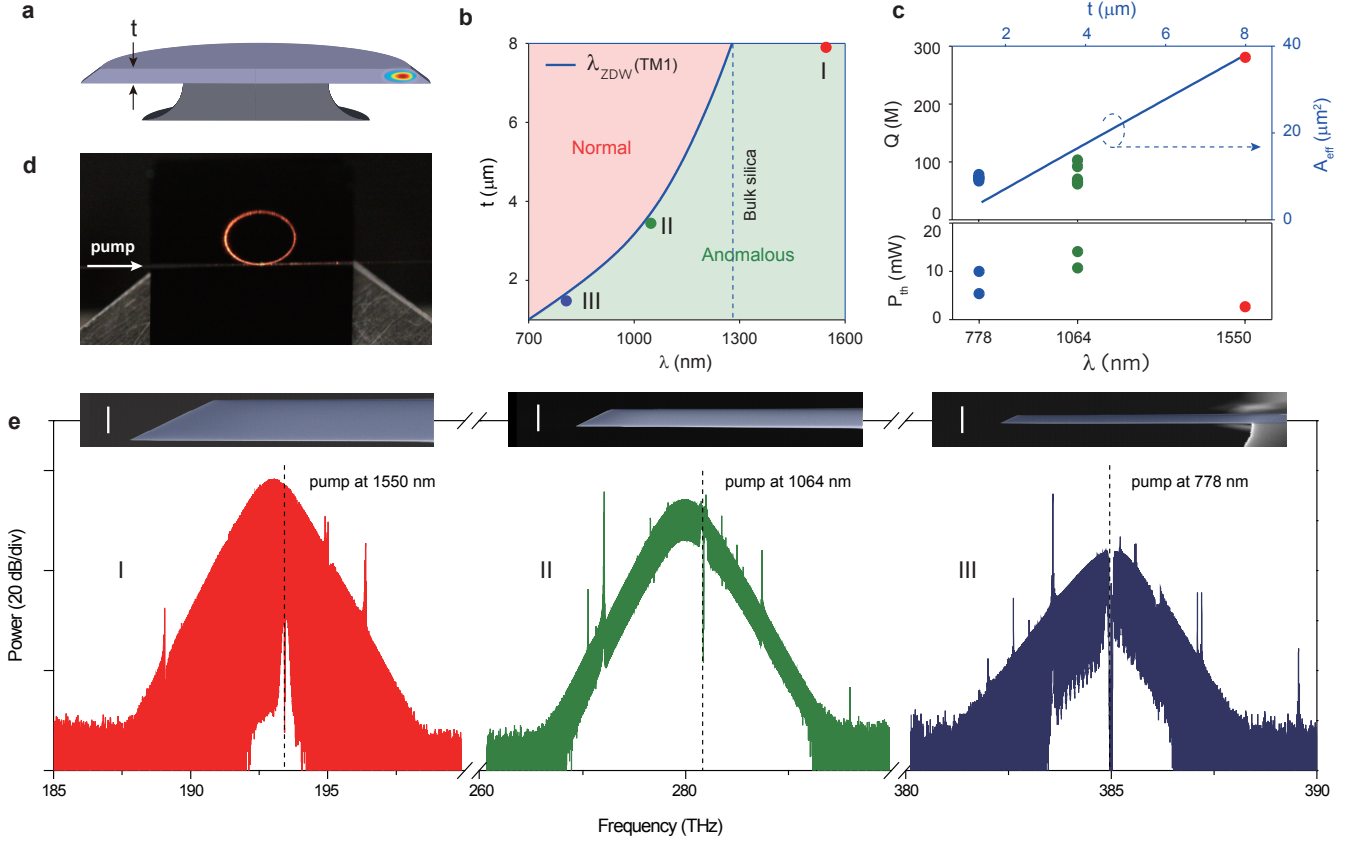


FIG. 1: Soliton frequency comb generation in dispersion-engineered silica resonators A rendering of a silica resonator with the calculated mode profile of the TM1 mode superimposed. (b) Regions of normal and anomalous dispersion are shown versus silica resonator thickness (t) and pump wavelength. The zero dispersion wavelength (λ_{ZDW}) for the TM1 mode appears as a blue curve. Plot is made for a 3.2-mm-diameter silica resonator. Three different device types I, II, and III are indicated for soliton generation at 1550 nm, 1064 nm and 778 nm. These correspond to three oxide thicknesses (t). (c) Measured Q factors and comb threshold powers versus thickness and pump wavelength for the three device types. Effective mode area (A_{eff}) of the TM1 mode family is also plotted as a function of wavelength and thickness. (d) A photograph of a silica resonator (Type III device pumped at 778 nm) while generating a soliton stream. The pump light is coupled via a tapered fiber from the left side of the resonator. The red light along the circumference of the resonator and at the right side of the taper is due to the short wavelength components of the soliton comb. (e) Soliton frequency comb spectra measured using device types I, II, and III designed for pump wavelengths 1550 nm, 1064 nm, and 778 nm, respectively. Pump frequency location is indicated by a dashed vertical line. The soliton pulse repetition rate of all devices is about 20 GHz. Insets: cross-sectional SEM images of the fabricated resonators. White scale bar is 5 μm .

optical-loss window so that optical Q factors can be high at short wavelengths. Here we demonstrate soliton microcombs with pump wavelengths of 1064 nm and 778 nm. These are the shortest soliton microcomb wavelengths demonstrated to date. By engineering geometric dispersion and by employing mode hybridization, net anomalous dispersion has been achieved at these wavelengths while also maintaining high optical Q factors (80 million at 778 nm, 90 million at 1064 nm). The devices have large (millimeter-scale) diameters and produce single soliton pulse streams at rates that are both detectable and processible by low-cost electronic circuits. Besides illustrating the flexibility of silica for soliton microcomb

generation across a range of short wavelengths, these results are relevant to potential secondary time standards at 778 nm based on the two-photon clock-transition in rubidium². Using dispersive-wave engineering in silica it might also be possible to extend the emission of these combs into the ultra-violet as has been recently demonstrated in compact silica waveguides³⁵.

The silica resonator used in this work is shown schematically in Fig. 1a. A fundamental mode profile is overlaid in the cross-sectional rendering. As described in detail below, the resonator thickness (t) is controlled to obtain net anomalous dispersion at the design wavelengths. The resonator design is a variation on the wedge

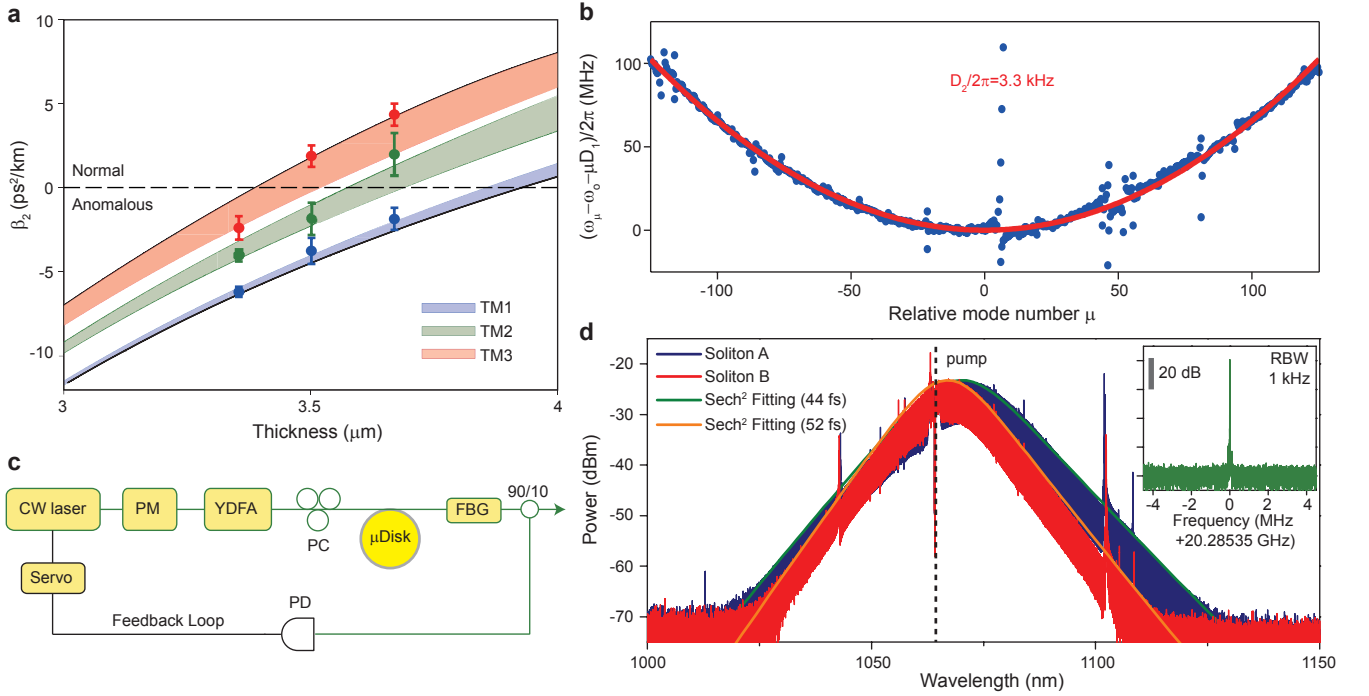


FIG. 2: Microresonator dispersion engineering and soliton generation at 1064 nm. (a) Simulated dispersion (GVD) of TM mode families versus resonator thickness. The angle of the wedge ranges from 30° to 40° in the colored regions. Measured data points are indicated and agree well with the simulation. (b) Measured mode frequency dispersion (blue points) versus relative mode number of a soliton-forming TM1 mode family in a 3.4 μm thick resonator. The red curve is a parabolic fit yielding $D_2/2\pi = 3.3$ kHz. (c) Experimental setup for soliton generation. A continuous-wave (CW) fiber laser is modulated by an electro-optic phase modulator (PM) before coupling to a ytterbium-doped-fiber-amplifier (YDFA). The pump light is then coupled to the resonator using a tapered fiber. Part of the comb power is used to servo-lock the pump laser frequency. FBG: fiber Bragg grating. PD: photodetector. PC: polarization controller. (d) Optical spectra of solitons at 1064 nm generated from the mode family shown in a. The two soliton spectra correspond to different power levels with the blue spectrum being a higher power and wider bandwidth soliton. The dashed vertical line shows the location of the pump frequency. The solid curves are sech² fittings. Inset: typical detected electrical beatnote showing soliton repetition rate. RBW: resolution bandwidth.

resonator and precise thickness control (t-control) is possible because this layer is formed through oxidation of a silicon wafer. The diameter of all resonators in this work (and the assumed diameter in all simulations) is 3.2 mm, which corresponds to a free-spectral-range (FSR) of approximately 20 GHz. Further details on fabrication are given elsewhere³⁹. As an aside, we note that a waveguide-integrated version of this design is also possible⁴⁰. Adaptation of that device using the methods described here would enable full integration with other photonic elements on the silicon chip.

Fig. 1b illustrates the dispersion design space by showing regions of resonator thickness t and pumping wavelength required to achieve anomalous dispersion for the TM1 mode family. The plot shows that as the pump wavelength decreases the resonator needs to be thinner to access the anomalous dispersion regime. With this in mind, we have selected three different device types for soliton frequency comb operation at three different pump

wavelengths. These are indicated in Fig. 1b as I, II and III with colored dots. At a pump wavelength of 1550 nm, the anomalous dispersion window is wide because bulk silica possesses anomalous dispersion at wavelengths above 1270 nm. For this device (Type I), an 8-μm thickness was used. Devices of type II and III have thicknesses near 3.5 μm and 1.5 μm for operation with pump wavelengths of 1064 nm and 778 nm, respectively. Measured Q factors for the three device types are plotted in the upper panel of Fig. 1c. Maximum Q factors at thicknesses which also produce anomalous dispersion were: 280 million (Type I, 1550 nm), 90 million (Type II, 1064 nm) and 80 million (Type III, 778 nm).

Using these three designs, soliton frequency combs were successfully generated with low threshold pump power. Shown in Fig. 1d is a photograph of a type III device. Soliton frequency components in the 700 nm band generate the red light in the photograph. Fig. 1e shows optical spectra of the soliton microcombs generated for

each device type. A slight Raman-induced soliton self-frequency-shift is observable in the type I and type II devices^{7,41–43}. Scanning electron microscope (SEM) images appear as insets in Fig. 1e and provide cross-sectional views of the three device types. It is worthwhile to note that microcomb threshold power, expressed as $P_{th} \sim A_{eff}/\lambda_p Q^2$ (λ_p is pump wavelength and A_{eff} is effective mode area) remains within a close range of powers for all devices (lower panel of Fig. 1c). This can be understood to result from partial compensation of reduced Q factor in the shorter wavelength devices by reduced optical mode area (see plot in Fig. 1c). For example, from 1550 nm to 778 nm the mode area is reduced by roughly a factor of 9 and this helps to offset a decrease in Q factor of 3X. The resulting P_{th} increase (5.4 mW at 778 nm versus approximately 2.5 mW at 1550 nm) is therefore caused primarily by the decrease in pump wavelength λ_p . In the following sections additional details on the device design, dispersion and experimental techniques used to generate these solitons are presented.

Dispersion simulations for TM modes near 1064 nm are presented in Fig. 2a and show that TM modes with anomalous dispersion occur in silica resonators having oxide thicknesses less than 3.7 μm . Aside from the thickness control, a secondary method to manipulate dispersion is by changing the wedge angle (see Fig. 2a). Here, wedge angles between 30 and 40 degrees were chosen in order to maximize the Q factors. Simulations also show that these angles minimize avoided-mode-crossings. The resonator dispersion is characterized by measuring mode frequencies using a scanning external-cavity-diode-laser (ECDL) whose frequency is calibrated using a Mach-Zehnder interferometer. As described elsewhere^{6,7} the mode frequencies, ω_μ , are Taylor expanded to second order as $\omega_\mu = \omega_o + \mu D_1 + \mu^2 D_2/2$, where ω_o denotes the pumped mode frequency and $D_1/2\pi$ is the FSR. D_2 is related to the GVD by $D_2 = -cD_1^2\beta_2/n_o$ where c and n_o are the speed of light and material refractive index, respectively. The measured frequency spectrum of the TM1 mode family in a 3.4 μm thick resonator is plotted in Fig. 2b. Also shown is a fitted parabola (red curve) revealing $D_2/2\pi = 3.3$ kHz (positive parabolic curvature indicates anomalous dispersion). The dispersion measured in resonators of different thicknesses, marked as solid dots in Fig. 2a, shows good agreement with numerical simulations.

The experimental setup is shown in Fig. 2c. The microresonator is pumped by a CW laser amplified by a YDFA. The pump light and comb power are coupled to and from the resonator by a tapered fiber. Solitons are generated while scanning the laser from higher frequencies to lower frequencies across the pump mode^{6–8}. The pump light is modulated by an electro-optic PM to overcome the thermal transient during soliton generation^{7,8,44}. A servo control referenced to the soliton power is employed to capture and stabilize the solitons⁴⁴. Shown in Fig. 2d are the optical spectra of solitons pumped at 1064 nm. These solitons are gener-

ated using the mode family whose dispersion is characterized in Fig. 2b. Due to the relatively low dispersion (small D_2), these solitons have a short temporal pulsewidth. Using the hyperbolic-secant-squared fitting method (see orange and green curves in Fig. 2d) a soliton pulse width of 52 fs is estimated for the red spectrum. By increasing the soliton power (blue spectrum) the soliton can be further compressed to 44 fs, which corresponds to a duty cycle of 0.09% at the 20 GHz repetition rate. Finally, the inset in Fig. 2d shows the electrical spectrum of the photodetected soliton pulse stream. Besides confirming the repetition frequency, the spectrum is very stable with excellent signal-to-noise ratio (SNR) greater than 70 dB.

For soliton operation near the pump wavelength 778 nm, a resonator thickness around 1.5 μm is chosen, which is close to the zero GVD of the TM1 mode (see Fig. 1b). Operation at this point provides thicker oxide and therefore higher optical Q factors. Under normal circumstances the near-zero GVD would prove challenging to control during fabrication, so mode coupling is used to engineer the dispersion^{31,32}. Specifically, the anomalous dispersion of the TM1 mode is boosted through hybridization with the TE2 mode. As now shown, this mode hybridization is caused by two factors: a degeneracy in the effective index at the pump wavelength of the two modes and a broken reflection symmetry of the resonator⁴⁶. Finite element method (FEM) simulation in Fig. 3a shows that at 778 nm the TM1 and TE2 modes are expected to have the same effective index at the thickness 1.48 μm when the resonator features a symmetry upon reflection through a plane that is both parallel to the resonator surface and that lies at the center of the of resonator. Such a symmetry exists when the resonator has vertical sidewalls or equivalently a wedge angle $\theta = 90^\circ$ in the current resonator design. A zoom-in of the effective index crossing is provided in Fig. 3b. In this symmetrical case, the two modes cross in the effective-index plot without hybridization. However, in the case of $\theta = 40^\circ$ (Fig. 3c), the symmetry is broken and the point of effective index degeneracy does not exist. Instead, near the resonator thickness 1.48 μm , two hybrid modes exist and these modes experience an avoided crossing. The avoided crossing causes a sudden transition in the calculated group velocity dispersion as shown in Fig. 3d. One of the hybrid modes experiences enhanced anomalous dispersion which allows for greater overall resonator thickness and hence higher resonator Q factors.

To verify this effect, resonators with three different thicknesses were fabricated and their dispersion was characterized using the same method as for the 1064 nm soliton device. The measured dispersion values are plotted as solid circles in Fig. 3d. Around the thickness 1.48 μm , the mode spectra of the two modes features significant higher-order dispersion (β_3 and β_4). Fig. 3e and Fig. 3f show the measured dispersion spectra of the two modes for devices with $t = 1.47$ μm and $t = 1.49$ μm , respectively. A zoom-in of the mode spectrum of the TM1

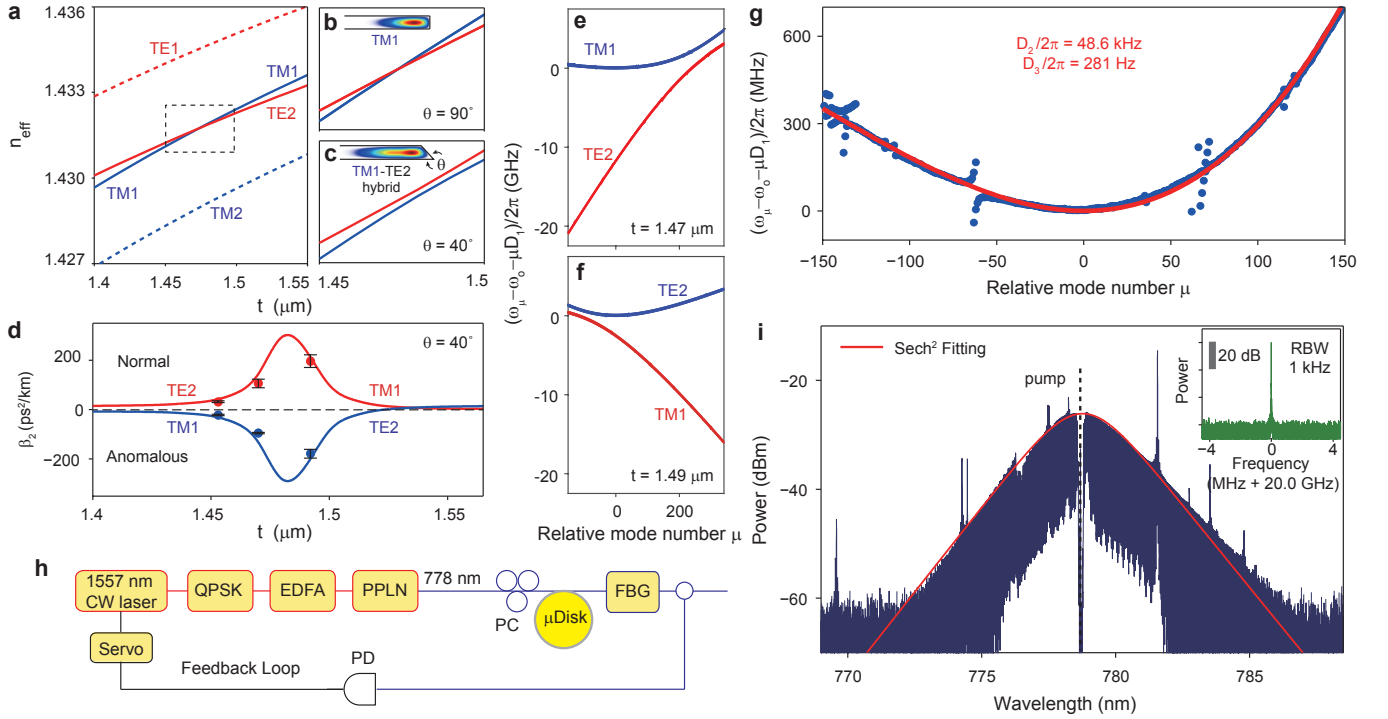


FIG. 3: Dispersion engineering and soliton generation at 778 nm (a) Calculated effective indices for TE1, TE2, TM1, and TM2 modes at 778 nm plotted versus thickness for a silica resonator with reflection symmetry. The TM1 and TE2 modes cross each other without hybridization. The dashed box is the frame for the panel **b** zoom-in. (b) Zoom-in of the dashed box in panel **a**. Inset shows resonator with reflection symmetry (equivalent to wedge angle $\theta = 90^\circ$). (c) As in **b** but for resonator with $\theta = 40^\circ$. An avoided crossing of TM1 and TE2 occurs due to mode hybridization. (d) Calculated GVD of the two hybrid modes for $\theta = 40^\circ$. Hybridization causes an abrupt transition in the dispersion around the thickness $1.48 \mu\text{m}$. The points are the measured dispersion values. (e, f) Measured mode frequencies of the TM1 and TE2 mode families versus relative mode number μ for devices with $t = 1.47 \mu\text{m}$ and $t = 1.49 \mu\text{m}$. (g) Zoom-in of panel **e** for the TM1 mode family. The red curve is a fit with $D_2/2\pi = 48.6 \text{ kHz}$ and $D_3/2\pi = 281 \text{ Hz}$. (h) Experimental setup for soliton generation. A 1557 nm tunable laser is sent to a quadrature phase shift keying modulator (QPSK) to utilize frequency-kicking⁴⁵ and is then amplified by an erbium-doped-fiber-amplifier (EDFA). Then, a periodically poled lithium niobate (PPLN) waveguide frequency doubles the 1557 nm input into 778 nm output. The 778 nm pump light is coupled to the resonator for soliton generation. A servo loop is used to maintain pump locking⁴⁴. (i) Optical spectrum of a 778 nm soliton with pump line indicated. The red curve is a spectral fitting which reveals the pulse width of 145 fs. Inset shows the electrical spectrum of the detected soliton pulse stream.

mode for $t = 1.47 \mu\text{m}$ with a fit (red curve) is shown in Fig. 3g. Despite the third-order dispersion, this dispersion curve is well suited for soliton formation.

For soliton generation, the microresonator is pumped at 778 nm by frequency-doubling from a CW ECDL operating at 1557 nm (see Fig. 3h). The 1557 nm laser is modulated by a QPSK modulator for frequency-kicking⁴⁵ and then amplified by an EDFA. The amplified light is sent into a PPLN device for second-harmonic generation. The frequency-doubled output pump power at 778 nm is coupled to the microresonator using a tapered fiber. The soliton capture and locking method was again used to stabilize the solitons⁴⁴. The optical spectrum of a 778 nm pumped soliton is shown in Fig. 3i. It features a temporal pulse width of 145 fs as derived from a sech^2 fit (red curve). The electrical spectrum of the photode-

tected soliton stream is provided as the inset to Fig. 3i and exhibits high stability.

In summary, we have demonstrated soliton microcombs at 778 nm and 1064 nm using on-chip high-Q silica resonators. Material-limited normal dispersion, which is dominant at these wavelengths, was compensated by using geometric dispersion through control of the resonator thickness and wedge angle. At the shortest wavelength, 778 nm, mode hybridization was also utilized to achieve anomalous dispersion while maintaining high optical Q. These results are the shortest wavelength soliton microcombs demonstrated to date. The generated solitons have pulse repetition rates of 20 GHz at both wavelengths. Such detectable and electronics-compatible repetition rate soliton microcombs at these short wavelengths have direct applications in optical

clocks³, metrology and spectroscopy^{4,5}. It is also possible that these results can be applied in optical coherence tomography^{47–49}. These same dispersion control methods should be transferable to silica ridge resonator designs that contain silicon nitride waveguides for on-chip coupling to other photonic devices⁴⁰. Also, it could be possible to design devices that use solitons formed at either 778 nm or 1064 nm for dispersive-wave generation into the visible and potentially into the ultraviolet as has been recently demonstrated using straight silica waveguides³⁵.

Acknowledgment The authors gratefully acknowledge

the Defense Advanced Research Projects Agency under the ACES program (Award No. HR0011-16-C-0118) and the SCOUT program (Award No. W911NF-16-1-0548). The authors also thank the Kavli Nanoscience Institute.

Author contributions SHL, DYO, QFY, BS, HW and KV conceived the experiment. SHL fabricated devices with assistance from DYO, BS, HW and KYY. DYO, QFY, BS and HW tested the resonator structures with assistance from SHL, KYY, YHL and XY. SHL, DYO, QFY, BS and HW modeled the device designs. All authors analyzed the data and contributed to writing the manuscript.

- ¹ Kippenberg, T. J., Holzwarth, R. & Diddams, S. A. Microresonator-based optical frequency combs. *Science* **332**, 555–559 (2011).
- ² Frank, I. *et al.* A low-power, chip-scale optical atomic clock with enhanced stability. In *Joint Navigation Conference* (2017).
- ³ Ludlow, A. D., Boyd, M. M., Ye, J., Peik, E. & Schmidt, P. O. Optical atomic clocks. *Reviews of Modern Physics* **87**, 637 (2015).
- ⁴ Diddams, S. A., Hollberg, L. & Mbele, V. Molecular fingerprinting with the resolved modes of a femtosecond laser frequency comb. *Nature* **445**, 627–630 (2007).
- ⁵ Ideguchi, T. *et al.* Coherent Raman spectro-imaging with laser frequency combs. *Nature* **502**, 355–358 (2013).
- ⁶ Herr, T. *et al.* Temporal solitons in optical microresonators. *Nature Photonics* **8**, 145–152 (2014).
- ⁷ Yi, X., Yang, Q.-F., Yang, K. Y., Suh, M.-G. & Vahala, K. Soliton frequency comb at microwave rates in a high-Q silica microresonator. *Optica* **2**, 1078–1085 (2015).
- ⁸ Brasch, V. *et al.* Photonic chip-based optical frequency comb using soliton cherenkov radiation. *Science* **351**, 357–360 (2016).
- ⁹ Wang, P.-H. *et al.* Intracavity characterization of micro-comb generation in the single-soliton regime. *Optics Express* **24**, 10890–10897 (2016).
- ¹⁰ Joshi, C. *et al.* Thermally controlled comb generation and soliton modelocking in microresonators. *Optics Letters* **41**, 2565–2568 (2016).
- ¹¹ Yang, Q.-F., Yi, X., Yang, K. Y. & Vahala, K. Stokes solitons in optical microcavities. *Nature Physics* **13**, 53–57 (2017).
- ¹² Spencer, D. T. *et al.* Towards an integrated-photonics optical-frequency synthesizer with <1 Hz residual frequency noise. In *Optical Fiber Communication Conference, M2J.2* (2017).
- ¹³ Suh, M.-G., Yang, Q.-F., Yang, K. Y., Yi, X. & Vahala, K. J. Microresonator soliton dual-comb spectroscopy. *Science* **354**, 600–603 (2016).
- ¹⁴ Dutt, A. *et al.* On-chip dual comb source for spectroscopy. *arXiv preprint arXiv:1611.07673* (2016).
- ¹⁵ Pavlov, N. *et al.* Soliton dual frequency combs in crystalline microresonators. *Optics Letters* **42**, 514–517 (2017).
- ¹⁶ Papp, S. B. & Diddams, S. A. Spectral and temporal characterization of a fused-quartz-microresonator optical frequency comb. *Physical Review A* **84**, 053833 (2011).
- ¹⁷ Li, Q. *et al.* Stably accessing octave-spanning microresonator frequency combs in the soliton regime. *Optica* **4**, 193–203 (2017).
- ¹⁸ Pfeiffer, M. H. *et al.* Octave-spanning dissipative Kerr soliton frequency combs in Si₃N₄ microresonators. *arXiv preprint arXiv:1701.08594* (2017).
- ¹⁹ Luke, K., Okawachi, Y., Lamont, M. R., Gaeta, A. L. & Lipson, M. Broadband mid-infrared frequency comb generation in a Si₃N₄ microresonator. *Optics Letters* **40**, 4823–4826 (2015).
- ²⁰ Savchenkov, A. A. *et al.* Generation of Kerr combs centered at 4.5 μ m in crystalline microresonators pumped with quantum-cascade lasers. *Optics Letters* **40**, 3468–3471 (2015).
- ²¹ Yu, M., Okawachi, Y., Griffith, A. G., Lipson, M. & Gaeta, A. L. Mode-locked mid-infrared frequency combs in a silicon microresonator. *Optica* **3**, 854–860 (2016).
- ²² Hugi, A., Villares, G., Blaser, S., Liu, H. & Faist, J. Mid-infrared frequency comb based on a quantum cascade laser. *Nature* **492**, 229–233 (2012).
- ²³ Coddington, I., Newbury, N. & Swann, W. Dual-comb spectroscopy. *Optica* **3**, 414–426 (2016).
- ²⁴ Saha, K. *et al.* Broadband parametric frequency comb generation with a 1- μ m pump source. *Optics Express* **20**, 26935–26941 (2012).
- ²⁵ Xue, X. *et al.* Second-harmonic-assisted four-wave mixing in chip-based microresonator frequency comb generation. *Light: Science & Applications* **6**, e16253 (2017).
- ²⁶ Jung, H., Stoll, R., Guo, X., Fischer, D. & Tang, H. X. Green, red, and IR frequency comb line generation from single IR pump in AlN microring resonator. *Optica* **1**, 396–399 (2014).
- ²⁷ Wang, L. *et al.* Frequency comb generation in the green using silicon nitride microresonators. *Laser & Photonics Reviews* **10**, 631–638 (2016).
- ²⁸ Hausmann, B., Bulu, I., Venkataraman, V., Deotare, P. & Lončar, M. Diamond nonlinear photonics. *Nature Photonics* **8**, 369–374 (2014).
- ²⁹ Riemensberger, J. *et al.* Dispersion engineering of thick high-Q silicon nitride ring-resonators via atomic layer deposition. *Optics Express* **20**, 27661–27669 (2012).
- ³⁰ Okawachi, Y. *et al.* Bandwidth shaping of microresonator-based frequency combs via dispersion engineering. *Optics*

- Letters* **39**, 3535–3538 (2014).
- ³¹ Liu, Y. *et al.* Investigation of mode coupling in normal-dispersion silicon nitride microresonators for Kerr frequency comb generation. *Optica* **1**, 137–144 (2014).
 - ³² Ramelow, S. *et al.* Strong polarization mode coupling in microresonators. *Optics Letters* **39**, 5134–5137 (2014).
 - ³³ Grudinin, I. S. & Yu, N. Dispersion engineering of crystalline resonators via microstructuring. *Optica* **2**, 221–224 (2015).
 - ³⁴ Yang, K. Y. *et al.* Broadband dispersion-engineered microresonator on a chip. *Nature Photonics* **10**, 316–320 (2016).
 - ³⁵ Oh, D. Y. *et al.* Coherent ultra-violet to near-infrared generation in silica ridge waveguides. *Nature Communications* **8**, 13922 (2017).
 - ³⁶ Kippenberg, T. J., Spillane, S. M. & Vahala, K. J. Kerr-nonlinearity optical parametric oscillation in an ultrahigh-Q toroid microcavity. *Physical Review Letters* **93**, 083904 (2004).
 - ³⁷ Moss, D. J., Morandotti, R., Gaeta, A. L. & Lipson, M. New CMOS-compatible platforms based on silicon nitride and Hydex for nonlinear optics. *Nature Photonics* **7**, 597–607 (2013).
 - ³⁸ Xiong, C. *et al.* Aluminum nitride as a new material for chip-scale optomechanics and nonlinear optics. *New Journal of Physics* **14**, 095014 (2012).
 - ³⁹ Lee, H. *et al.* Chemically etched ultrahigh-Q wedge-resonator on a silicon chip. *Nature Photonics* **6**, 369–373 (2012).
 - ⁴⁰ Yang, K. Y. *et al.* Integrated ultra-high-Q optical resonator. *ArXiv e-prints* (2017). 1702.05076.
 - ⁴¹ Milián, C., Gorbach, A. V., Taki, M., Yulin, A. V. & Skryabin, D. V. Solitons and frequency combs in silica microring resonators: Interplay of the Raman and higher-order dispersion effects. *Physical Review A* **92**, 033851 (2015).
 - ⁴² Karpov, M. *et al.* Raman self-frequency shift of dissipative Kerr solitons in an optical microresonator. *Physics Review Letters* **116**, 103902 (2016).
 - ⁴³ Yi, X., Yang, Q.-F., Yang, K. Y. & Vahala, K. Theory and measurement of the soliton self-frequency shift and efficiency in optical microcavities. *Optics Letters* **41**, 3419–3422 (2016).
 - ⁴⁴ Yi, X., Yang, Q.-F., Yang, K. Y. & Vahala, K. Active capture and stabilization of temporal solitons in microresonators. *Optics Letters* **41**, 2037–2040 (2016).
 - ⁴⁵ Stone, J. R. *et al.* Initiating Kerr-soliton frequency combs apart from thermal bistability and mode perturbation effects. In *Conference on Lasers and Electro-Optics*, STu4J.4 (2017).
 - ⁴⁶ Dai, D. & Bowers, J. E. Novel concept for ultracompact polarization splitter-rotator based on silicon nanowires. *Optics Express* **19**, 10940–10949 (2011).
 - ⁴⁷ Lee, S.-J., Widiyatmoko, B., Kourogi, M. & Ohtsu, M. Ultrahigh scanning speed optical coherence tomography using optical frequency comb generators. *Japanese Journal of Applied Physics* **40**, L878 (2001).
 - ⁴⁸ Kray, S., Spöler, F., Först, M. & Kurz, H. Dual femtosecond laser multiheterodyne optical coherence tomography. *Optics Letters* **33**, 2092–2094 (2008).
 - ⁴⁹ Bajraszewski, T. *et al.* Improved spectral optical coherence tomography using optical frequency comb. *Optics Express* **16**, 4163–4176 (2008).